

Excitons in one-dimensional Mott insulators

F.H.L. Essler¹, F. Gebhard² and E. Jeckelmann²

¹ *Department of Physics, Warwick University, Coventry, CV4 7AL, UK*

² *Fachbereich Physik, Philipps-Universität Marburg, D-35032 Marburg, Germany*

We employ dynamical density-matrix renormalization group (DDMRG) and field-theory methods to determine the frequency-dependent optical conductivity in one-dimensional extended, half-filled Hubbard models. The field-theory approach is applicable to the regime of “small” Mott gaps which is the most difficult to access by DDMRG. For very large Mott gaps the DDMRG recovers analytical results obtained previously by means of strong-coupling techniques. We focus on exciton formation at energies below the onset of the absorption continuum. As a consequence of spin-charge separation, these Mott-Hubbard excitons are bound states of spinless, charged excitations (“holon-antiholon” pairs). We also determine exciton binding energies and sizes. In contrast to simple band insulators, we observe that excitons exist in the Mott-insulating phase only for a sufficiently strong intersite Coulomb repulsion. Furthermore, our results show that the exciton binding energy and size are not related in a simple way to the strength of the Coulomb interaction.

PACS numbers: 71.10.Fd, 71.35.Cc, 72.80.Sk

I. INTRODUCTION

Excitons in conventional band insulators are well-described by Wannier theory¹. A Wannier exciton is a charge neutral optical excitation made of an electron in the conduction band and a hole in the valence band, bound together by the Coulomb attraction between them. In inorganic semiconductors like GaAs the typical binding energy, as defined by the energy difference between the exciton and the band edge of the particle-hole continuum, is several meV. This should be compared to the band gap itself, which is of the order of one eV. Concomitantly the typical size of a Wannier exciton is of the order of 100 Å, which is almost two orders of magnitude larger than the lattice spacing. We note that although the total spin of an optically excited exciton is necessarily zero, it is composed of two quasiparticles carrying spin-1/2.

In quasi one-dimensional materials like conjugated polymers² the situation is quite different. Here the electron-electron interaction accounts, to a substantial degree, for the optical gap itself³ as well as for the formation of excitons. The exciton binding energy in, e.g., polydiacetylenes is found to be of the order of 0.5 eV^{4,5} and is thus comparable to the optical gap of 2.4 eV in 3BCMU-polydiacetylene chains diluted in their monomer matrix^{4,5}. The exciton size was estimated⁵ to be 12 Å and is thus comparable to the length of the unit cell of 5 Å. These facts suggest that electron-electron interactions will play an important role in any theoretical description of excitons in these materials.

Realistic models for conjugated polymers must account for the effects of both electron-electron and electron-phonon interactions. The interplay between these makes the reliable calculation of the optical conductivity a very demanding task. As a first step it is therefore natural to investigate the effects of the two mechanisms separately⁶. The optical conductivity for models with

only electron-lattice coupling such as the celebrated Su-Schrieffer-Heeger model has been widely analyzed in the literature⁷ and is well established. As an extension of this approach, electron-electron interactions have been taken into account perturbatively⁸. In contrast there are comparatively few reliable results for the optical spectrum in models that take account of the sizable electron-electron interaction^{9–12}. The interaction drives these systems into a Mott-insulating ground state¹³. The scarcity of results is due to the difficulties associated with the calculation of excited state properties in one-dimensional Mott insulators. Therefore, it is of considerable interest to develop reliable methods for the investigation of optical excitations in correlated electron systems, and to determine the optical conductivity of one-dimensional Mott insulators.

In this paper we focus on the calculation of the optical conductivity in models with electron-electron interactions only. We study an extended Hubbard model with nearest and next-nearest neighbor density-density interactions; the model is further specified in Sec. II.

We employ two recently developed numerical and analytical techniques to determine the real part of the optical conductivity over the full frequency range and analyze exciton properties without suffering from finite-size limitations; for a first application to the Hubbard model, see Ref. 14. In Sec. III we first test the dynamical density-matrix renormalization group (DDMRG) by applying it to the limit of large Mott gaps where analytical results are available¹⁵. We obtain excellent agreement between numerical and analytical results, and confirm the clear and simple physical picture of an exciton as a bound state of a double occupancy and an empty lattice site in a background of singly occupied sites. We then move on to the generic case of intermediate Mott gaps and find qualitatively the same physical behavior.

In the regime of small Mott gaps, finite-size effects and finite resolution of the DDMRG start to hamper the nu-

merical analysis. Therefore, in Sec. IV, we carry out a weak-coupling field-theory analysis of the problem. Using the form-factor bootstrap approach we determine the optical conductivity in the field-theory limit. Here, the spin sector does not couple to the current operator so that it is sufficient to analyze the charge sector only. The exciton is then described as a bound state of a holon and an antiholon, which are the elementary charge excitations in the theory. The resulting picture for small Mott gaps remains very similar to the cases of intermediate to large gaps. We even find quantitative agreement between field theory and DDMRG results for intermediate Mott gaps where the applicability of field theory is not a priori expected.

In Sec. V we discuss two fundamental properties of Mott–Hubbard excitons, their binding energy and size, in greater detail. In contrast to Wannier excitons in band insulators, Mott–Hubbard excitons exist only when the intersite Coulomb repulsion exceeds a certain threshold. In general, the exciton binding energy is not related in a simple way to the strength of the Coulomb interaction. We analyze a new correlation function which allows to define the size of an exciton in correlated electron systems. Our analysis provides a comprehensive picture of excitons in one-dimensional Mott insulators.

In our conclusions (Sec. VI) we address implications of our results for the theory of π -conjugated polymers.

II. MODEL HAMILTONIAN

In this work we study the one-dimensional extended Hubbard model¹⁶,

$$\begin{aligned} \hat{H} = & -t \sum_{l,\sigma} \left(\hat{c}_{l,\sigma}^+ \hat{c}_{l+1,\sigma} + \hat{c}_{l+1,\sigma}^+ \hat{c}_{l,\sigma} \right) \\ & + U \sum_l \left(\hat{n}_{l,\uparrow} - \frac{1}{2} \right) \left(\hat{n}_{l,\downarrow} - \frac{1}{2} \right) \\ & + V_1 \sum_l (\hat{n}_l - 1)(\hat{n}_{l+1} - 1) \\ & + V_2 \sum_l (\hat{n}_l - 1)(\hat{n}_{l+2} - 1). \end{aligned} \quad (1)$$

This Hamiltonian describes electrons with spin $\sigma = \uparrow, \downarrow$ which can hop between neighboring sites. Here $\hat{c}_{l,\sigma}^+$, $\hat{c}_{l,\sigma}$ are creation and annihilation operators for electrons with spin σ at site l , $\hat{n}_{l,\sigma} = \hat{c}_{l,\sigma}^+ \hat{c}_{l,\sigma}$ are the corresponding number operators, and $\hat{n}_l = \hat{n}_{l,\uparrow} + \hat{n}_{l,\downarrow}$.

Since we are interested in the Mott insulating phase, we exclusively consider a half-filled band where the number of electrons N equals the number of lattice sites L . The lattice spacing is set to unity, $a_0 \equiv 1$. Note that we have chosen the chemical potential in such a way that the Hamiltonian explicitly exhibits a particle-hole symmetry. This Hamiltonian has two other discrete symmetries which are useful for optical excitation calculations:

a spin-flip symmetry and a spatial-reflection symmetry (through the lattice center). Therefore, each eigenstate of (1) has a well-defined parity under charge conjugation ($P_c = \pm 1$) and spin flip ($P_s = \pm 1$), and belongs to one of the two irreducible representations, A_g or B_u , of a one-dimensional lattice reflection symmetry group.

The kinetic energy is diagonal in momentum space and gives rise to a cosine band, $\epsilon(k) = -2t \cos(k)$ of width $W = 4t$. The Coulomb repulsion is mimicked by a repulsive, local Hubbard interaction U , and nearest and next-nearest neighbor repulsions V_1 , V_2 . We restrict ourselves to the physically relevant case $U > V_1 > V_2 \geq 0$. In this work, we are not interested in issues like a complete classification of the phase diagram of the model (1); instead, we constrain our analysis to the consideration of several different points in the Mott insulating phase. A more systematic investigation of the extended Hubbard model with $V_2 = 0$ will be published elsewhere¹⁷. There it is shown that without the next-nearest neighbor interaction, it is not possible to have simultaneously a small Mott gap and form a Mott–Hubbard exciton.

Linear optical absorption is one of the most commonly used probes in experimental studies of the dynamical properties of a material. The optical absorption is proportional to the real part of the optical conductivity, which is related to the imaginary part of the current-current correlation function by

$$\sigma_1(\omega > 0) = \frac{\text{Im}\{\chi(\omega > 0)\}}{\omega}, \quad (2a)$$

$$\chi(\omega > 0) = -\frac{1}{L} \langle 0 | \hat{j} \frac{1}{E_0 - \hat{H} + \hbar\omega + i\eta} \hat{j} | 0 \rangle \quad (2b)$$

$$= -\frac{1}{L} \sum_n \frac{|\langle 0 | \hat{j} | n \rangle|^2}{\hbar\omega - (E_n - E_0) + i\eta}. \quad (2c)$$

Here, $|0\rangle$ is the ground state, $|n\rangle$ are excited states, and E_0 , E_n are their respective energies. Although $\eta = 0^+$ is infinitesimal, we may introduce a finite value to broaden our resonances at $\hbar\omega = E_n - E_0$. In momentum space, the current operator reads

$$\hat{j} = -\frac{2et}{\hbar} \sum_{k;\sigma} \sin(k) \hat{c}_{k,\sigma}^+ \hat{c}_{k,\sigma}. \quad (3)$$

We note that the current operator is invariant under the spin-flip transformation but antisymmetric under charge conjugation and spatial reflection. Therefore, if the ground state $|0\rangle$ belongs to the symmetry subspace (A_g, P_c, P_s), only excited states $|n\rangle$ belonging to the symmetry subspace ($B_u, -P_c, P_s$) contribute to the optical conductivity. According to selection rules, the matrix element $\langle 0 | \hat{j} | n \rangle$ vanishes if $|n\rangle$ belongs to another symmetry subspace. We set $\hbar = 1$ throughout, and for the presentation of our results we use $e = t \equiv 1$ in our figures.

III. DENSITY-MATRIX RENORMALIZATION GROUP

Recently, the density-matrix renormalization group method^{18,19} (DMRG) has been extended to the calculation of *dynamical* correlation functions^{12,14,20}. This numerical technique allows us to obtain $\sigma_1(\omega)$ for all interaction strengths as long as the gap is not exponentially small. A complete exposition of our DDMRG method will be published elsewhere²¹.

DDMRG allows us to calculate dynamical correlation functions, such as the r.h.s. of (2b), very accurately over the full frequency range for fairly large systems ($L \leq 128$) with open boundary conditions and a *finite* broadening factor η , i.e., the DDMRG actually gives

$$\sigma_{\eta;L}(\omega) = \frac{1}{L} \sum_n \frac{|\langle 0 | \hat{j} | n \rangle|^2}{E_n - E_0} \frac{\eta}{[\omega - (E_n - E_0)]^2 + \eta^2} . \quad (4)$$

For $\eta \rightarrow 0$, $\sigma_{\eta;L}(\omega)$ reduces to $\sigma_1(\omega)$ as defined in Eq. (2). Ultimately, we are interested in the optical conductivity of an infinite system, $L \rightarrow \infty$, for $\eta \rightarrow 0^+$. It is shown in Ref. 21 that the most appropriate way of approaching this double limit is to compute $\sigma_{\eta;L}(\omega)$ for different system sizes while keeping $\eta L = \text{const}$ and then to extrapolate to infinite system size. In this paper we use $\eta L = 12.8t$, which yields an energy resolution of $0.1t$ for our largest system size ($L = 128$).

A very useful consistency check of the method is to test various sum rules, relating moments of the function $\sigma_1(\omega)$ to ground-state expectation values, which can be evaluated with great accuracy using a standard DMRG method^{18,19}. For instance, for the Hamiltonian (1) with open boundary conditions

$$\int_0^\infty \frac{d\omega}{\pi} \omega \sigma_1(\omega) = \frac{1}{L} \langle 0 | \hat{j}^2 | 0 \rangle, \quad (5a)$$

$$\int_0^\infty \frac{d\omega}{\pi} \sigma_1(\omega) = \frac{e^2 t}{2L} \langle 0 | \sum_{l;\sigma} \left(\hat{c}_{l,\sigma}^+ \hat{c}_{l+1,\sigma} + \text{h.c.} \right) | 0 \rangle, \quad (5b)$$

$$\int_0^\infty \frac{d\omega}{\pi} \frac{\sigma_1(\omega)}{\omega} = \frac{e^2}{L} \langle 0 | \left[\sum_l l (\hat{n}_l - 1) \right]^2 | 0 \rangle . \quad (5c)$$

For $\sigma_{\eta;L}(\omega)$ these sum rules are not fulfilled exactly, but only up to errors of the order of $\mathcal{O}([\eta/t])$ or $\mathcal{O}([\eta/t]^2)$.

The ground-state phase diagram of the Hamiltonian (1) exhibits several different phases (for instance, Mott-Hubbard insulator, charge density wave, and bond-order wave for $U > V_1 \geq 0$ and $V_2 = 0$, see Ref. 17). To check the nature of the ground state for some fixed model parameters we calculate the spin gap and various ground state properties, such as charge density, bond order, and spin and density correlations, for large system sizes (up to $L = 512$ sites) with a standard DMRG method. The ground state of (1) is a Mott insulator for all values of the model parameters used in this work.

With DMRG one can also calculate the charge gap

$$E_c(L) = E_0(L+1) + E_0(L-1) - 2E_0(L), \quad (6)$$

where $E_0(N)$ is the ground state energy of (1) on a L -site lattice with N electrons. For $L \rightarrow \infty$, E_c gives the energy threshold of the electron-hole excitation continuum. In a Mott insulator it corresponds to the Mott gap. In the one-dimensional Hubbard model ($V_1 = V_2 = 0$), it is known that E_c is also equal to the optical gap which we define as the energy threshold of the lowest band in the optical spectrum. In all cases with $V_1, V_2 \neq 0$ discussed here we have found that the optical spectrum contains a single band, which corresponds to unbound particle-hole excitations, and that E_c agrees with the onset of this band. Therefore, in this paper we identify the charge gap with the optical gap. (Some special cases for which the charge gap does not correspond to the optical gap are discussed in Ref. 17.)

We also use the symmetrized DMRG method²² to calculate the lowest eigenstates in the optical excitation symmetry subspace (see Sec. II). As the standard DMRG method, the symmetrized DMRG yields not only the eigenenergies but also allows us the computation of various expectation values and correlation functions of the eigenstates (for an example, see Sec. V). We can thus investigate the nature and properties of these optical excitations. In particular, it is possible to distinguish unbound particle-hole excitations from excitons and from other kinds of excitations (excitonic strings, charge-density-wave droplets) which can dominate the optical spectrum of a Mott insulator¹⁷. In this paper we consider only the regime of the Hamiltonian (1) where optically excited states can be described as (bound or unbound) particle-hole pairs. We emphasize that the symmetrized DMRG results for the optically excited states are always in perfect agreement with the DDMRG results for the optical conductivity, confirming the accuracy of both methods.

All DMRG methods have a truncation error which is reduced by increasing the number m of retained density matrix eigenstates (for more details, see Refs. 18,19). Varying m allows one to compute physical quantities for different truncation errors and thus to obtain error estimates on these quantities. For some quantities, especially eigenenergies, it is possible to extrapolate the results to the limit of vanishing truncation error and thus to achieve a greater accuracy. We have systematically used these procedures to estimate the precision of our numerical calculations and adjusted the maximal number m of density matrix eigenstates to reach a desired accuracy. The largest number of density matrix eigenstates we have used is $m = 1200$. For all numerical results presented in this paper DMRG truncation errors are negligible unless specified explicitly. The main cause of inaccuracies are finite size effects or extrapolation errors for $L \rightarrow \infty$ which we discuss below when we present our numerical results.

A. Limit of large Mott gaps

Let us now consider the situation where the Mott gap is much larger than the band width $4t$. For large interaction strengths, $U \gg t, V_1, V_2$, it is possible to analyze the model (1) by means of a $1/U$ expansion¹⁵. If we ignore corrections of the order t/U , all sites are singly occupied in the ground state. Electron transfers are limited to processes that conserve the number of double occupancies, and a rather simple band picture emerges for $V_1 = V_2 = 0$. In an optical absorption process we excite one hole at momentum $k - q/2$ in the lower Hubbard band, $\epsilon_{\text{LHB}}(k) = -U/2 + \epsilon(k)$, and one double occupancy at momentum $k + q/2$ in the upper Hubbard band, $\epsilon_{\text{UHB}}(k) = U/2 - \epsilon(k)$ (antiparallel bands). The total momentum of the two charge excitations is q , and their energy is ω . Due to spin-charge separation, the oscillator strength can be written as¹⁵

$$|\langle 0 | \hat{j} | n \rangle|^2 = |-ie\epsilon(k)|^2 g_q. \quad (7)$$

The spin sector enters the current-current correlation function via the momentum-dependent ground-state form factor g_q ,

$$g_q = 2 \langle 0 | \hat{Z}_{r,r+1}^+(q) \left(\frac{1}{4} - \hat{\mathbf{S}}_r \cdot \hat{\mathbf{S}}_{r+1} \right) \hat{Z}_{r,r+1}(q) | 0 \rangle \quad (8a)$$

$$\hat{Z}_{r,r+1}(q) = \frac{1}{L} \sum_l e^{-iqL} \hat{T}_S^{(l-r)} \hat{T}_{S'}^{(l-r)}, \quad (8b)$$

where \hat{T}_S shifts all spins by one site whereas $\hat{T}_{S'}$ performs the same operation on the lattice with sites r and $r+1$ removed.

For the large- U Hubbard model itself, the analysis of g_q is rather involved. We can use a “no-recoil approximation”¹⁵ to argue that the dominant contributions to the conductivity come from $q = 0$ and $q = \pi$, which correspond to vertical transitions between two antiparallel bands ($q = 0$; $\epsilon_{\text{LHB}}(k)$, $\epsilon_{\text{UHB}}(k)$) and between two parallel bands ($q = \pi$; $\epsilon_{\text{LHB}}(k)$, $\epsilon_{\text{UHB}}(k + \pi)$). This hypothesis has subsequently been confirmed by DDMRG^{14,17}, which yields excellent agreement if the form factors are chosen as $g_0 = 2.65$ and $g_\pi = 0.05 \pm 0.03$. Exact sum rules impose the condition $g_0 + g_\pi = 4 \ln(2) \approx 2.77$ for an infinite system. The deviation of our best fits can be traced back to finite-size effects and numerical errors of the order of one percent.

We now discuss the effects of a finite nearest-neighbor Coulomb repulsion $V_1 \ll U$ with $V_2 = 0$. It follows by direct inspection of the Hamiltonian (1) that the double occupancy and the hole now mutually attract. To some extent, this is reminiscent of the situation encountered in Wannier theory for a band insulator. However, unlike in Wannier theory, the double occupancy and the hole are not fermionic quasi-particles but spinless hard-core bosons. Even more importantly, there is a critical value $V_c = 2t$ below which no exciton appears

below the threshold of the particle-hole continuum at $\omega_{\text{ph}} = E_c = U - 4t$. For $V_1 > V_c$ there is an exciton at the energy

$$\omega_1 = U - V_1 - 4t^2/V_1. \quad (9a)$$

In addition, there is a second Mott-Hubbard exciton at the energy

$$\omega_2 = U - V_1, \quad (9b)$$

which, for $V_1 < 4t$, lies in the particle-hole continuum but carries very little spectral weight.

The optical conductivity is given by

$$\begin{aligned} \omega \sigma_1(\omega) = & \pi g_\pi t^2 e^2 \delta(\omega - \omega_2) \\ & + g_0 t^2 e^2 \left\{ \Theta(V_1 - 2t) \pi \left(1 - (2t/V_1)^2 \right) \delta(\omega - \omega_1) \right. \\ & \left. + \Theta(4t - |\omega - U|) \frac{2t^2 \sqrt{1 - ((\omega - U)/4t)^2}}{V_1(\omega - \omega_1)} \right\}. \end{aligned} \quad (10)$$

Here, $\Theta(x)$ is the Heaviside step function. Apart from the two δ -peaks corresponding to the excitons, there is a particle-hole continuum for $|\omega - U| \leq 4t$. Near the lower (upper) boundary, the optical conductivity shows a characteristic square-root increase (decrease). The only exception is the case of $V_1 = V_c$ where the optical conductivity diverges at the threshold,

$$\sigma_1(\omega) \propto \frac{1}{\sqrt{\omega - \omega_{\text{ph}}}} \quad \text{for } \omega - \omega_{\text{ph}} \rightarrow 0^+ \quad (V_1 = 2t). \quad (11)$$

The predictions of this strong-coupling analysis are confirmed by our numerical results. Note that $\sigma_1(\omega) \sim 1/U$ so that it is more convenient in DDMRG to calculate directly the imaginary part of the current-current correlation function, i.e., $\text{Im} \{ \chi(\omega) \} = \omega \sigma_1(\omega)$. In analogy to Eq. (4), a broadening η is introduced in the DDMRG procedure for the current-current correlation function,

$$\text{Im} \{ \chi_{\eta;L}(\omega) \} = \frac{1}{L} \sum_n \frac{\eta |\langle 0 | \hat{j} | n \rangle|^2}{[\omega - (E_n - E_0)]^2 + \eta^2}. \quad (12)$$

For $\eta \rightarrow 0$, this expression reduces to $\text{Im} \{ \chi(\omega) \}$, and we analyze the finite-size effects as discussed above for $\sigma_1(\omega)$.

Figure 1 shows $\text{Im} \{ \chi_{\eta;L}(\omega) \}$ for $L = 128$ and $\eta = 0.1t$ obtained in the large- U limit of the extended Hubbard model with $V_1 = 5t$ and $V_2 = 0$. We compare the DDMRG data to the analytical formula (10), convolved with a Lorentzian of width η . The DDMRG data and the large- U result are in very good agreement when we choose $g_0 = 2.65$, $g_\pi = 0.08$, as discussed above. These values are found to be essentially independent of V_1 . We previously obtained a similarly good agreement for the case of the large- U Hubbard model ($V_1 = V_2 = 0$)¹⁴.

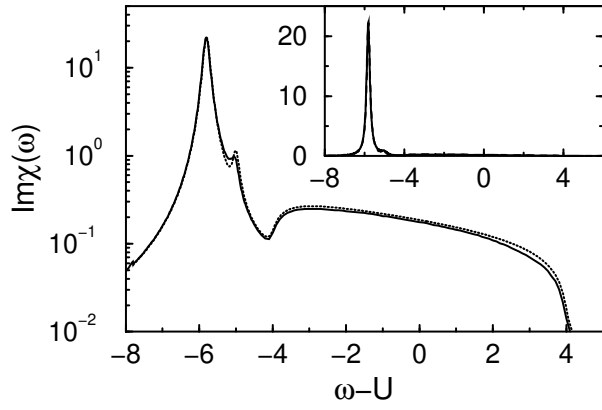


FIG. 1. Current-current correlation function $\text{Im}\{\chi(\omega)\}$ for $U/t \rightarrow \infty$, $V_1 = 5t$, $V_2 = 0$, and $\eta = 0.1t$. The solid line is the DDMRG result $\text{Im}\{\chi_{\eta;L}(\omega)\}$ for $L = 128$. The dotted line is Eq. (10) convolved with a Lorentzian of width η . Note the logarithmic scale of the ordinate. Inset: same results on a linear scale.

For $V_1 = 5t$, $V_2 = 0$, most of the spectral weight is carried by the exciton at $\omega - U = \omega_1 - U = -5.8t$, as one also observes for typical band insulators. Therefore we use a logarithmic scale to make visible the contributions of the other exciton and the particle-hole continuum. The use of a logarithmic scale also reveals deviations around the second exciton ($\omega - U \approx \omega_2 - U = -5t$) and close to the upper band edge ($\omega - U \approx +4t$), which are associated with difficulties in the numerical determination of small contributions to the optical spectrum, and remaining finite-size and boundary effects. In fact, these deviations are less than one percent of the total spectral weight, and are completely irrelevant for practical, i.e., experimental purposes. On a linear scale they are not visible as seen in the inset of Fig. 1.

The case of $0 < V_2 < V_1$ can be treated analogously and does not yield any new physical aspects. It is known that increasing the interaction range simply reduces the critical coupling below which no exciton appears in the gap and increases the number of visible excitons in the spectrum²³.

B. Regime of intermediate Mott gaps

In the simple Hubbard model ($V_1 = V_2 = 0$) we previously found that the optical conductivity evolved smoothly from the regime of small Mott gaps ($U \ll t$) to the limit of large Mott gaps ($U \gg t$)¹⁴. Optical excitations can simply be interpreted as a particle-hole pair, i.e., a pair of spinless quasi-particles with opposite charges, corresponding to the hole and double occupancy for large Mott gaps and to the holon-antiholon pair in the field-theory limit of small Mott gaps (see Sec. IV).

The optical spectrum of the extended Hubbard model (1) shows more diversity in the presence of a finite intersite Coulomb repulsion ($V_1 > V_2 \geq 0$). Even within

the Mott insulator phase one can observe “exotic” optical excitations such as charge-density-wave droplets or excitonic strings¹⁷. In this study we restrict ourselves to the Mott insulator regime of (1) where the dominant optical excitations can be described as a (bound or unbound) particle-hole pair and the Coulomb interaction is strong enough to generate at least one bound pair (exciton).

Varying the model parameters U/t , V_1/t , and V_2/t we have investigated the optical excitations of systems with a Mott gap ranging from 10 to 0.1 times the band width $4t$. It is important to note that the Mott gap E_c increases with U and V_2 but decreases with increasing V_1 ^{11,17,24}. As in the large Mott gap limit, we have found that the intersite Coulomb interaction must exceed a critical value before a discrete absorption peak appears at an energy ω_{ex} below the optical gap E_c . For $V_2 = 0$ the critical value is $V_1 \approx 2t$ for all U/t in agreement with our analytical strong-coupling analysis and a previous work²⁵. The critical value of V_1/t becomes smaller as the next-nearest neighbor repulsion V_2 increases.

We have analyzed the nature of the excited states associated with the discrete absorption peak using various measurements and correlation functions. For instance, in Sec. VB we present a method to determine the size of a particle-hole pair. This analysis confirms that this excited state is clearly a bound particle-hole pair (exciton). The exciton binding energies $\delta E = E_c - \omega_{\text{ex}}$ observed in our calculations range from $\delta E = 0.03t$ to $\delta E = 12t$ and the exciton sizes measured with the procedure of Sec. VB vary from $20a_0$ down to slightly more than one lattice spacing.

It is interesting to note that we have never found more than one exciton in the regime of intermediate Mott gaps. Our numerical results (DDMRG and symmetrized DMRG) for finite open chains sometimes yield more than one optical excitations with energy $\omega_q \approx \omega_{\text{ex}} + c(L)q^2 < E_c$ and quasi-momenta $q \approx \pi(2\ell + 1)/(L + 1)$, $\ell = 0, 1, 2, \dots, \ell_{\text{max}} \ll L/2$.²⁶ The first of these states ($\ell = 0$) has always much more spectral weight than the other ones and corresponds to an exciton with momentum $q = 0$ in an infinite chain. Scattering by the chain ends is responsible for the small but finite optical weight of the other states ($\ell \geq 1$), corresponding to excitons with momentum $q \neq 0$ in an infinite system. Thus, with periodic boundary conditions or in an infinite system, only one exciton contributes to the optical conductivity $\sigma_1(\omega)$ of the Hamiltonian (1) in the regime of intermediate Mott gaps.

In contrast to this, both the strong-coupling analysis and field theory allow for more than one exciton in the optical spectrum of a Mott insulator in the thermodynamic limit if the Coulomb repulsion becomes strong enough. For the model (1) an increase of V_1 and V_2 does not lead to the formation of a second Mott-Hubbard exciton. Instead, the nature of the lowest optical excitations changes to charge-density-wave droplets or excitonic strings, or the ground state develops long-range

order. Both the strong-coupling analysis and the field-theory approach assume a Mott insulator ground state and particle-hole pairs as optical excitations, and thus do not reproduce this instability toward charge density ordering. It is conceivable, though, that the inclusion of Coulomb terms beyond next-nearest neighbors in the lattice model (1) favors the appearance of more excitons in the optical conductivity of a Mott insulator.

Besides the single exciton peak we have always found that $\sigma_1(\omega)$ shows an absorption band starting at the charge gap E_c . Within the resolution of our method the optical spectrum does not display any other feature. The investigation of the excited states in the continuum above E_c is much more demanding than the analysis of the isolated exciton peak. Whenever this has been feasible, we have found that the excited states contributing to the absorption continuum can be described as an unbound particle-hole pair (see Sec. VB).

As a typical example, the optical conductivity of (1) for $U = 8t$, $V_1 = 4t$, and $V_2 = 2t$ is shown in Fig. 2. A peak at the exciton energy $\omega_{\text{ex}} = 3.34t$ is the dominant feature of the spectrum while a very weak band is visible for $\omega \geq E_c = 4.05t$. No gap is visible between ω_{ex} and E_c because of the broadening of the strong exciton peak. In the inset of Fig. 2 one can see the weak particle-hole continuum part of the spectrum separated from the strong exciton contribution. The onset of the absorption band is clearly visible at $\omega \approx E_c = 4.05t$. The small irregular fluctuations seen in the inset are numerical errors (truncation errors) made visible by the small scale used.

In summary, our numerical results show that there is no qualitative change in the optical conductivity of a Mott insulator with excitons when one goes from the limit of large Mott gaps down to the regime of intermediate Mott gaps with $E_c \gtrsim 0.4t$. As in the Hubbard model¹⁴, the simple picture of the strong-coupling analysis remains qualitatively valid.

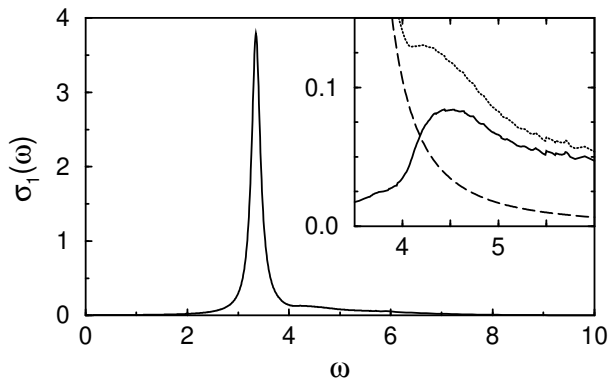


FIG. 2. Optical conductivity $\sigma_{\eta;L}(\omega)$ for $U = 8t$, $V_1 = 4t$, and $V_2 = 2t$, calculated with DDMRG on a 128-site lattice ($\eta = 0.1t$). The inset shows an expanded view of $\sigma_{\eta;L}(\omega)$ (dotted line) for $3.5 \leq \omega/t \leq 6$. The exciton (dashed) and continuum (solid) contributions to $\sigma_{\eta;L}(\omega)$ are also shown.

IV. FIELD THEORY

In order to address the regime of small Mott gaps, we study the extended Hubbard model (1) in the field-theoretical limit. This limit can be constructed directly from the lattice model in the weak-coupling regime $U, V_1, V_2 \ll t$. The low-energy physics of the non-interacting model is simply described in terms of a massless Dirac fermion with velocity $v_F = 2ta_0$. The interactions introduce a four-fermion coupling. The resulting effective theory is known as the $U(1)$ Thirring model and can be represented as^{27,28}

$$\begin{aligned} \mathcal{H} &= \int dx [\mathcal{H}_c + \mathcal{H}_s], \\ \mathcal{H}_s &= \sum_{\alpha} \left\{ \frac{2\pi v_s}{3} [: J^{\alpha} J^{\alpha} : + : \bar{J}^{\alpha} \bar{J}^{\alpha} :] - 2g_{\perp} J^{\alpha} \bar{J}^{\alpha} \right\}, \\ \mathcal{H}_c &= \sum_{\alpha} \frac{2\pi v_c}{3} [: I^{\alpha} I^{\alpha} : + : \bar{I}^{\alpha} \bar{I}^{\alpha} :] \\ &\quad + [g_{\perp} (I^x \bar{I}^x + I^y \bar{I}^y) + g_{\parallel} I^z \bar{I}^z], \end{aligned} \quad (13)$$

where J^{α} , \bar{J}^{α} (I^{α} , \bar{I}^{α}) are left and right moving $SU(2)$ spin currents ($SU(2)$ pseudospin currents) and

$$\begin{aligned} g_{\perp} &= 2(U - 2[V_1 - V_2])a_0, \quad g_{\parallel} = 2(U + 6V_1 + 2V_2)a_0, \\ v_c &= v_F + \frac{2(U/4 + V_1 + V_2)a_0}{\pi}, \quad v_s = v_F - \frac{Ua_0}{2\pi}. \end{aligned} \quad (14)$$

The Hamiltonian (13) explicitly exhibits spin-charge separation: $\mathcal{H}_{c,s}$ describe the charge and spin degrees of freedom, respectively, which are independent of one another. As long as $g_{\perp} > 0$, the spin sector remains gapless and can be bosonized in terms of a Gaussian model. The charge sector can be bosonized as well, as is for example shown in Ref. 27. The result is a Sine-Gordon model (SGM)

$$\mathcal{H}_c = \frac{1}{16\pi} [(\partial_t \phi_c)^2 + (v_c \partial_x \phi_c)^2] + 2\mu_c \cos \beta \phi_c, \quad (15)$$

where μ_c and β are functions of U , V_1 , V_2 . In order to utilize results obtained from the integrability of the Sine-Gordon model we use a flat renormalization scheme, in which β is a constant

$$\beta^2 = \frac{4\pi v_F}{4\pi v_F + \sqrt{g_{\parallel}^2 - g_{\perp}^2}}. \quad (16)$$

The pure Hubbard model corresponds to the limit $\beta \rightarrow 1$ and the effect of V_1 and V_2 is to decrease the value of β .

In the field-theory limit the electrical current operator is found to be

$$\mathcal{J}(t, x) = \sqrt{A'} \partial_t \phi_c, \quad (17)$$

where $A' > 0$ is a non-universal constant. As seen from Eq. (17), the current operator does not couple to the spin

sector. This shows that spinons do not contribute to the optical conductivity. Therefore we ignore the spin part \mathcal{H}_s of the Hamiltonian from now on.

The calculation of the optical conductivity in the field-theory limit has thus been reduced to the evaluation of the retarded current-current correlation function in the charge sector,

$$\chi^{\text{FT}}(\omega) = \frac{i}{La_0} \int_0^\infty dt \exp(i\omega t) \int_{-\infty}^\infty dx \langle [\mathcal{J}(x, t), \mathcal{J}(0, 0)] \rangle. \quad (18)$$

We turn to the calculation of this correlation function in Sec. IV A.

For the Sine-Gordon model, many exact results are available²⁹. The spectrum of the SGM depends on the value of the coupling constant β . In the so-called repulsive regime, $1/\sqrt{2} < \beta < 1$, there are only two elementary excitations, called soliton and antisoliton. From the point of view of the underlying lattice model (1) these correspond to holon and antiholon (spinless excitations of opposite charges). These have a massive relativistic dispersion,

$$E(P) = \sqrt{M^2 + v_c^2 P^2}, \quad (19)$$

where M is the single-particle gap which is related to the optical gap by $\Delta = 2M$. At weak coupling the gap scales as

$$M \approx \frac{8t}{\sqrt{2\pi}} \sqrt{g(1+x)} \left(\frac{1-x}{1+x} \right)^{(gx+2)/4gx}, \quad (20)$$

where we have fixed the constant factor by comparing to the exact result for the Hubbard model, and where

$$x = \left[1 - \left(\frac{U - 2V_1 + 2V_2}{U + 6V_2 + 2V_2} \right)^2 \right]^{1/2}, \quad (21)$$

$$g = (U + 6V_1 + 2V_2)/2\pi t.$$

We note that the gap vanishes on the critical surface $U - 2V_1 + 2V_2 = 0$ separating the Mott-insulating phase with gapless spin excitations from another phase with a spin gap.

In the regime $0 < \beta < 1/\sqrt{2}$, soliton and antisoliton attract and can form bound states. In the SGM these are usually known as “breathers” and correspond to excitons in our lattice model. There are

$$N_{\text{ex}} = \left\lceil \frac{1 - \beta^2}{\beta^2} \right\rceil \quad (22)$$

different types of excitons, where $[x]$ in (22) denotes the integer part of x . The exciton gaps are given by

$$M_n = 2M \sin(n\pi\xi/2), \quad n = 1, \dots, N_{\text{ex}}, \quad (23)$$

where

$$\xi = \frac{\beta^2}{1 - \beta^2}. \quad (24)$$

Therefore, the single-particle gap M and the coupling β fully characterize the spectrum of the SGM.

One knows that the field-theory approximation to the lattice problem is valid in the limit $U, V_1, V_2 \ll t$ where the single-particle gap is much smaller than the bandwidth. For the Hubbard model ($V_1 = V_2 = 0$) we have found¹⁴ that field theory gives surprisingly good results for the optical conductivity even for intermediate single-particle gaps of magnitude $M \approx 0.3t$. The same holds true for the Mott insulating phase of the extended Hubbard model with $V_1 > 0$, $V_2 = 0$ ^{17,30}. As we shall show in Sect. IV B, field theory remains applicable even in the presence of excitons.

In the framework of the field-theory approximation to the lattice problem we can determine the value of β only in the limit $U, V_1, V_2 \ll t$. In fact, for the Hubbard model $\beta = 1$ is fixed by the $\text{SO}(4)$ symmetry³¹. As seen from Eq. (16), the effect of a small V_1, V_2 is to decrease the value of β . One may therefore hope that by carefully tuning U, V_1 and V_2 one may stay in a regime with a “small” single-particle gap, i.e., close to the critical surface $U - 2V_1 + 2V_2 = 0$, but with a sufficiently small β for excitons to exist. We have found numerically that it is indeed possible to reach regions of the parameter space where field theory is valid and β^2 is as small as 0.36 close to a critical surface $U - 2V_1 + 2V_2 \approx 0$ which separates the Mott insulating phase from other phases with long-range order. The determination of the field-theoretical parameter β^2 as a function of the lattice model parameters using DMRG results will be discussed in Sec. IV B.

A. Optical conductivity in the Sine-Gordon model

Our task is now to calculate the Fourier transform of the retarded, dynamical current-current correlation function (18) in the Sine-Gordon model. This is done by going to the spectral representation and then utilizing the integrability of the SGM to determine exactly the matrix elements of the current operator between the ground state and various excited states. This method is known as the form-factor bootstrap approach^{32,33} and has recently been applied to calculate the optical conductivity in the repulsive regime of the SGM^{14,30}. Here we review briefly the relevant steps and refer to Ref. 28 for a more detailed exposition. In order to utilize the spectral representation we need to specify a basis of eigenstates of the Hamiltonian (15). Such a basis is given by scattering states of excitons, holons and antiholons. In order to distinguish these we introduce labels $e_1, e_2, \dots, e_{N_{\text{ex}}}, h, \bar{h}$. As usual for particles with relativistic dispersion, it is useful to introduce a rapidity variable θ to parameterize energy and momentum

$$E_h(\theta) = M \cosh \theta, \quad P_h(\theta) = (M/v_c) \sinh \theta, \quad (25a)$$

$$E_{\bar{h}}(\theta) = M \cosh \theta, \quad P_{\bar{h}}(\theta) = (M/v_c) \sinh \theta, \quad (25b)$$

$$E_{e_n}(\theta) = M_n \cosh \theta, \quad P_{e_n}(\theta) = (M_n/v_c) \sinh \theta, \quad (25c)$$

where the exciton gaps M_n are given by (23). Next we turn to the construction of a basis of scattering states of holons, antiholons and excitons. A convenient formalism to this end is obtained by using the Zamolodchikov-Faddeev (ZF) algebra. The ZF algebra can be considered to be the extension of the algebra of creation and annihilation operators for free fermions or bosons to the case of interacting particles with factorizable scattering. The ZF algebra is based on the knowledge of the exact spectrum and scattering matrix of the model³⁴. For the SGM the ZF operators (and their hermitian conjugates) satisfy the following algebra

$$Z^{\epsilon_1}(\theta_1)Z^{\epsilon_2}(\theta_2) = S_{\epsilon'_1, \epsilon'_2}^{\epsilon_1, \epsilon_2}(\theta_1 - \theta_2)Z^{\epsilon'_2}(\theta_2)Z^{\epsilon'_1}(\theta_1), \quad (26a)$$

$$Z_{\epsilon_1}^\dagger(\theta_1)Z_{\epsilon_2}^\dagger(\theta_2) = Z_{\epsilon'_2}^\dagger(\theta_2)Z_{\epsilon'_1}^\dagger(\theta_1)S_{\epsilon_1, \epsilon_2}^{\epsilon'_1, \epsilon'_2}(\theta_1 - \theta_2), \quad (26b)$$

$$Z^{\epsilon_1}(\theta_1)Z_{\epsilon_2}^\dagger(\theta_2) = Z_{\epsilon'_2}^\dagger(\theta_2)S_{\epsilon_2, \epsilon_1}^{\epsilon'_2, \epsilon_1}(\theta_2 - \theta_1)Z^{\epsilon'_1}(\theta_1) + (2\pi)\delta_{\epsilon_2}^{\epsilon_1}\delta(\theta_1 - \theta_2). \quad (26c)$$

Here $S_{\epsilon'_1, \epsilon'_2}^{\epsilon_1, \epsilon_2}(\theta)$ are the known (factorizable) two-particle scattering matrices³⁴ and $\varepsilon_j = h, \bar{h}, e_1, \dots, e_{[1/\varepsilon]}$.

Using the ZF operators a Fock space of states can be constructed as follows. The vacuum is defined by

$$Z_{\varepsilon_i}(\theta)|0\rangle = 0. \quad (27)$$

Multiparticle states are then obtained by acting with strings of creation operators $Z_\epsilon^\dagger(\theta)$ on the vacuum

$$|\theta_n \dots \theta_1\rangle_{\epsilon_n \dots \epsilon_1} = Z_{\epsilon_n}^\dagger(\theta_n) \dots Z_{\epsilon_1}^\dagger(\theta_1)|0\rangle. \quad (28)$$

In term of this basis the resolution of the identity is given by

$$\mathbb{1} = |0\rangle\langle 0| + \sum_{n=1}^{\infty} \sum_{\epsilon_i} \int_{-\infty}^{\infty} \frac{d\theta_1 \dots d\theta_n}{(2\pi)^n n!} |\theta_n \dots \theta_1\rangle_{\epsilon_n \dots \epsilon_1} {}^{\epsilon_1 \dots \epsilon_n} \langle \theta_1 \dots \theta_n|. \quad (29)$$

Inserting (29) between the current operators in (18), we obtain the following spectral representation of the correlation function

$$\begin{aligned} \langle \mathcal{J}(x, t) \mathcal{J}(0, 0) \rangle &= \sum_{n=1}^{\infty} \sum_{\epsilon_i} \int \frac{d\theta_1 \dots d\theta_n}{(2\pi)^n n!} \\ &\times \exp\left(i \sum_{j=1}^n P_j x - E_j t\right) |\langle 0 | \mathcal{J}(0, 0) | \theta_n \dots \theta_1 \rangle_{\epsilon_n \dots \epsilon_1}|^2, \end{aligned} \quad (30)$$

where P_j and E_j are given by

$$P_j = \frac{M_{\epsilon_j}}{v_c} \sinh \theta_j, \quad E_j = M_{\epsilon_j} \cosh \theta_j, \quad (31)$$

and

$$f^{\mathcal{J}}(\theta_1 \dots \theta_n)_{\epsilon_1 \dots \epsilon_n} \equiv \langle 0 | \mathcal{J}(0, 0) | \theta_n \dots \theta_1 \rangle_{\epsilon_n \dots \epsilon_1} \quad (32)$$

are the form factors. Our conventions in (31) are such that $M_h = M_{\bar{h}} = M$ and $M_{e_n} = M_n$. After carrying out the double Fourier transform we arrive at

$$\begin{aligned} \chi^{\text{FT}}(\omega) &= \frac{-2\pi}{La_0} \sum_{n=1}^{\infty} \sum_{\epsilon_i} \int \frac{d\theta_1 \dots d\theta_n}{(2\pi)^n n!} |f^{\mathcal{J}}(\theta_1 \dots \theta_n)_{\epsilon_1 \dots \epsilon_n}|^2 \\ &\times \left[\frac{\delta(\sum_j M_{\epsilon_j} \sinh \theta_j / v_c)}{\omega - \sum_j M_{\epsilon_j} \cosh \theta_j + i\eta} - \frac{\delta(\sum_j M_{\epsilon_j} \sinh \theta_j / v_c)}{\omega + \sum_j M_{\epsilon_j} \cosh \theta_j + i\eta} \right]. \end{aligned} \quad (33)$$

This then yields the following representation for the real part of the optical conductivity ($\omega > 0$)

$$\begin{aligned} \sigma_1^{\text{FT}}(\omega) &= \frac{2\pi^2}{La_0 \omega} \sum_{n=1}^{\infty} \sum_{\epsilon_i} \int \frac{d\theta_1 \dots d\theta_n}{(2\pi)^n n!} \\ &\times |f^{\mathcal{J}}(\theta_1 \dots \theta_n)_{\epsilon_1 \dots \epsilon_n}|^2 \\ &\times \delta\left(\sum_k \frac{M_{\epsilon_k}}{v_c} \sinh \theta_k\right) \delta\left(\omega - \sum_k M_{\epsilon_k} \cosh \theta_k\right). \end{aligned} \quad (34)$$

The missing ingredient in (34) are the form factors. In Refs. 32,33 integral representations for the form factors of the current operator in the Sine-Gordon model were derived. Using these results we can determine the first few terms of the expansion (34). In particular, the form factors involving excitons are determined via the bootstrap axioms for soliton-antisoliton form factors³².

From (34) it is easy to see for any given frequency ω only a finite number of intermediate states will contribute: the delta function forces the sum of single-particle gaps $\sum_j M_{\epsilon_j}$ to be less than ω . Expansions of the form (34) are usually found to exhibit a rapid convergence, which can be understood in terms of phase space arguments^{35,36}. Therefore we expect that summing the first few terms in (34) will give us good results over a large frequency range.

Using the transformation property of the current operator under charge conjugation one finds that many of the form factors in (33) actually vanish. In particular, only the “odd” excitons e_1, e_3, \dots (assuming they exist, i.e., β is sufficiently small) couple to the current operator. The first few non-vanishing terms of the spectral representation (34) are

$$\frac{\sigma_1^{\text{FT}}(\omega)}{A} = \sum_{n=1}^{[(N_{\text{ex}}+1)/2]} \sigma_{e_{2n-1}}(\omega) + \sigma_{h\bar{h}}(\omega) + \sigma_{e_1 e_2}(\omega) + \dots \quad (35)$$

Here $A = A'v_c/La_0$ and $\sigma_{e_n}(\omega)$, $\sigma_{h\bar{h}}(\omega)$ and $\sigma_{e_1 e_2}(\omega)$ are the contributions of the odd excitons, the holon-antiholon

continuum and the $e_1 e_2$ exciton-exciton continuum respectively. The latter of course exists only if $N_{\text{ex}} \geq 2$. We find

$$\sigma_{e_n}(\omega) = \frac{\pi}{M_{2n-1}^2} f_{2n-1} \delta(\omega - M_{2n-1}) \quad (36a)$$

$$f_m = 4M^2 \xi^2 \sin(m\pi\xi) \prod_{n=1}^{m-1} \tan^2(\pi n\xi/2) \quad (36b)$$

$$\times \exp\left(-2 \int_0^\infty \frac{dt}{t} \frac{\sinh(t(1-\xi)/2)}{\sinh(t\xi/2) \cosh(t/2)} \frac{\sinh^2(mt\xi/2)}{\sinh t}\right).$$

The holon-antiholon contribution has previously been determined³⁰ and is given by

$$\sigma_{h\bar{h}}(\omega) = \frac{4\sqrt{\omega^2 - 4M^2}\Theta(\omega - 2M)}{\omega^2[\cos(\pi/\xi) + \cosh(\theta/\xi)]} \quad (37)$$

$$\times \exp\left(\int_0^\infty \frac{dt}{t} \frac{\sinh[t(1-\xi)/2] [1 - \cos(t\theta/\pi) \cosh t]}{\sinh(t\xi/2) \cosh(t/2) \sinh t}\right),$$

where $\theta = 2\text{arccosh}(\omega/2M)$. Finally, we quote the result for the $e_1 e_2$ exciton-exciton continuum

$$\sigma_{e_1 e_2}(\omega) = \frac{2\omega |f_{12}(\theta_{12})|^2}{\sqrt{(\omega^2 - M_1^2 - M_2^2)^2 - (2M_1 M_2)^2}}, \quad (38)$$

where

$$|f_{12}(\theta_{12})|^2 = \lambda^6 \frac{|\tan \pi\xi|}{2} \frac{\sinh^2 \theta_{12} + \sin^2(\pi\xi/2)}{\sinh^2 \theta_{12} + \sin^2(3\pi\xi/2)}$$

$$\times \exp\left(-8 \int_0^\infty \frac{dt}{t} \frac{\sinh t \sinh(t\xi) \sinh[t(1+\xi)] \cosh(2t\xi)}{\sinh^2(2t)}\right)$$

$$\times \exp\left(-4 \int_0^\infty \frac{dt}{t} \frac{\sinh(2t\xi) \sinh[t(1+\xi)] \cos(2t\theta_{12}/\xi)}{\cosh t \sinh(2t)}\right)$$

$$\times (4 \cos[2\pi(\cosh \theta_{12} + \cos(\pi\xi/2))/\xi])^{-2}, \quad (39)$$

and

$$\theta_{12} = \text{arccosh}\left(\frac{\omega^2 - M_1^2 - M_2^2}{2M_1 M_2}\right), \quad (40)$$

$$\lambda = 2 \cos\left(\frac{\pi\xi}{2}\right) \sqrt{2 \sin\left(\frac{\pi\xi}{2}\right) \exp\left(-\int_0^{\pi\xi} \frac{dt}{2\pi} \frac{t}{\sin t}\right)}.$$

For $1 \geq \beta^2 > 1/3$ the contributions of the first odd exciton (36) and of the holon-antiholon continuum (37) dominate the field-theoretical optical conductivity (35) (at least in the low-frequency regime) and other contributions vanish or can be neglected. The optical conductivity can be written as

$$\sigma_1^{\text{FT}}(\omega) = \frac{A}{\Delta} h_\beta\left(\frac{\omega}{\Delta}\right), \quad (41)$$

where $h_\beta(x)$ is a universal function depending only on β^2 . Therefore, only the parameter β^2 determines the shape of the optical spectrum. The parameters Δ and A/Δ just set the energy and conductivity scales, respectively.

For $1 \geq \beta^2 \geq 1/2$ the optical spectrum contains a single band, while for $1/2 > \beta^2 > 1/3$ it contains one band and one exciton peak in the optical gap at the energy $\omega_{\text{ex}} = M_1$. The optical weight is progressively transferred from the band to the single exciton as β^2 decreases down to $1/3$. The absorption band increases smoothly at the threshold Δ , as

$$\sigma_1^{\text{FT}}(\omega) \propto \sqrt{\omega - \Delta} \quad \text{for } \omega \rightarrow \Delta^+, \quad (42)$$

for all values of β^2 but $\beta^2 = 1/2$, when the exciton peak merges with the band. In this case $\sigma_1^{\text{FT}}(\omega)$ shows a square-root divergence at the absorption threshold

$$\sigma_1^{\text{FT}}(\omega) \propto \frac{1}{\sqrt{\omega - \Delta}} \quad \text{for } \omega \rightarrow \Delta^+ (\beta^2 = 1/2). \quad (43)$$

The behavior of the field-theoretical conductivity is thus qualitatively similar to that of the lattice model in the large Mott-gap limit (10). For $V_2 = 0$ ¹⁷ it has also been found for intermediate Mott gaps that $\sigma_1(\omega)$ diverges as a square-root at the absorption band threshold E_c for the critical coupling $V = V_c$ below which no exciton appears in the optical gap. For $V_1 \neq V_c$, $\sigma_1(\omega)$ increases smoothly at the absorption band threshold. This generic behavior of $\sigma_1(\omega)$ illustrates once more the absence of significant qualitative changes in the particle-hole continuum and single-exciton spectrum of (1) as one goes from the large to the small Mott gap limit. For $\beta^2 \leq 1/3$, the field-theoretical optical conductivity shows more features, but it seems that this regime cannot be reached in the lattice model (1) and thus we shall not discuss it further.

B. Application to the lattice model

The field theory optical conductivity $\sigma_1^{\text{FT}}(\omega)$, (Eq. 35), depends on three parameters: β^2 , the gap $\Delta = 2M$, and the normalization A . To compare the field theory predictions with our numerical results for the lattice model (1) one needs to determine the field theory parameters corresponding to specific values of the model parameters U , V_1 , and V_2 . Fortunately, if there is exactly one exciton in the spectrum ($1/2 > \beta^2 > 1/3$), this can be done using standard DMRG techniques.

The first step is the calculation of the gap parameter Δ . The gap Δ obviously corresponds to the charge gap (6) extrapolated to the infinite system limit, $\Delta = \lim_{L \rightarrow \infty} E_c(L)$. The second step is determining β^2 . The exciton energy $\omega_{\text{ex}}(L)$ of the lattice system can be calculated using the symmetrized DMRG method. The extrapolation to infinite system size gives us the exciton gap of field theory, Eq. (23), $M_1 = \lim_{L \rightarrow \infty} \omega_{\text{ex}}(L)$. The parameter β^2 is then fixed by the ratio of M_1 and $\Delta = 2M$ through Eqs. (23) and (24).

The final step is the calculation of the normalization A . Evaluating A accurately turns out to be the most difficult task and we have tried two different approaches. In the

first one we calculate the excitonic spectral weight in the lattice model using the symmetrized DMRG technique and extrapolate to an infinite system size. This yields the normalization A by comparison with the field-theory prediction, Eqs. (35) and (36). This method is simple and exact on the field theory side but difficult to carry out numerically because of significant truncation errors and complicated finite-size effects.

In the second approach we use the sum rules (5). We numerically integrate the contributions of the exciton and the holon-antiholon continuum to the optical conductivity (35) for a fixed value of β^2 . The result has a trivial dependence on A and Δ because of (41). This gives us the l.h.s. of (5b) or (5c) assuming that the neglected contributions to $\sigma_1^{\text{FT}}(\omega)$ are insignificant and that most of the optical spectrum weight is concentrated at low energy where field theory is expected to describe the lattice-model properties accurately. The r.h.s. of (5b) and (5c) can be calculated for the lattice model with DMRG and extrapolated to the infinite system limit. Comparison of both sides of the equations give the value of the normalization A .

We prefer the second approach because it is simpler and more accurate than the first one as far as the numerical calculations are concerned. It can also be used when there is no exciton ($1 \geq \beta^2 \geq 1/2$). Unfortunately, the second approach works only if the exciton (36) and holon-antiholon continuum (37) reproduce the lattice model $\sigma_1(\omega)$ very accurately, i.e., if

$$\delta S_n = \int_0^\infty d\omega \omega^{-n} |A \sigma_{e1}(\omega) + A \sigma_{h\bar{h}}(\omega) - \sigma_1(\omega)| \quad (44)$$

is very small compared to the l.h.s of (5b) for $n = 0$ or the l.h.s. of (5c) for $n = 1$.

The validity of the field-theory approximation to the model (1) is not necessarily restricted to the limit $U, V_1, V_2 \ll t$ but rather to the regions where the single-particle gap $M = \Delta/2 = E_c/2$ is small compared to the band width $4t$. In the Hubbard model¹⁴ ($V_1 = V_2 = 0$) we have found that field theory describes the optical conductivity accurately even for $U = 3t$, corresponding to $\Delta \approx 0.6t$. In the case $V_1 > 0, V_2 = 0$, field theory is valid not only in the weak-coupling limit ($U, V_1 \ll t$) but also in the vicinity of a critical line $U - 2V_1 \approx 0$ separating the Mott-insulating phase from phases with long-range order¹⁷. The Mott gap vanishes or becomes extremely small on this critical line at least up to $U = 4t$. The holon-antiholon continuum contribution (37) to the optical conductivity agrees with DDMRG results for gaps $\Delta \approx 0.6t$ and β^2 ranging from 1 to $1/2$.

In the general case ($U > V_1 > V_2 > 0$), there is also a critical surface $U - 2V_1 + 2V_2 \approx 0$ separating the Mott insulating phase from other phases (in particular, a charge-density-wave phase), where the Mott gap vanishes or becomes very small even for relatively strong Coulomb interaction (at least up to $U = 6t$). A careful tuning of the parameters U, V_1 , and V_2 allows one to reach regions of the parameter space, where field theory appears

to remain valid and β^2 decreases down to 0.36 (for instance, $U = 6t, V_1 = 4.5t$, and $V_2 = 2t$). We can thus compare our numerical results with the field-theoretical predictions for the optical conductivity in the parameter regime with a single exciton. Again, we have found a good agreement between DDMRG and field theory for gaps as large as $\Delta = 0.6t$.

In Fig. 3 we compare the optical conductivity from field theory and DDMRG for $U = 5.2t, V_1 = 3.7t$, and $V_2 = 1.3t$. Only the low-frequency ($\omega \leq 2t$) part of the spectrum is shown as there is almost no spectral weight at higher frequency. The numerical results have been calculated on a 128-site chain with a resolution of $\eta = 0.1t$. The field-theory result, Eqs. (35)–(37), has been convolved with a Lorentzian of width $\eta = 0.1t$ to allow for a direct comparison with DDMRG results. The field theory parameters $\Delta = 0.625t, \beta^2 = 0.40$, and $A = 1.12e^2t$ have been evaluated for an infinite chain as discussed above. The gap between the exciton peak at $M_1 = 0.544t$ and the threshold of a weak holon-antiholon continuum at Δ is not visible in Fig. 3 because it is smaller than the finite resolution introduced by the broadening.

In Fig. 3 one sees that the agreement between numerical and field-theory results is good. The visible discrepancies are well-understood finite-size effects: the excitation energies of (1), in particular the exciton energy, decreases as the system size increases, the total spectral weight is slightly smaller in the finite chain as shown by corrections to the kinetic energy (r.h.s. of (5b)) of the order $1/L$, and the exciton peak is broadened and flattened because of the scattering by chain ends. If we choose the field-theory parameters Δ and A (the energy and conductivity scales) to fit the finite-system DDMRG conductivity, differences almost completely vanish for $\Delta = 0.669t$ and $A = 1.02e^2t$, as seen in the inset of Fig. 3.

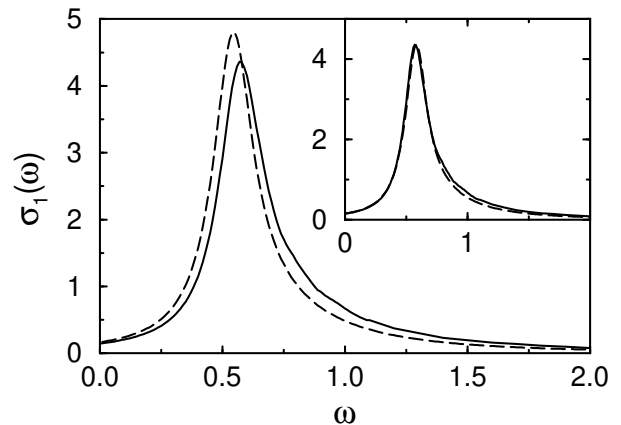


FIG. 3. Optical conductivity $\sigma_{\eta;L}(\omega)$ (solid) calculated with DDMRG for $U = 5.2t, V_1 = 3.7t$, and $V_2 = 1.3t$ on a 128-site lattice ($\eta = 0.1t$). Field-theoretical result $\sigma_1^{\text{FT}}(\omega)$ (dashed) for $\Delta = 0.625t, \beta^2 = 0.40$ and $A = 1.12e^2t$, convolved with a Lorentzian of width $\eta = 0.1t$. Inset: same results with $\Delta = 0.669t$ and $A = 1.02e^2t$.

As mentioned in Sec. IIIB we have never observed more than one exciton below the optical absorption continuum in the regime of intermediate Mott gaps, down to $E_c = 0.4t$. Therefore, we cannot evaluate the field-theory predictions for the additional excitons and the exciton-exciton continuum in the regime $\beta^2 \leq \frac{1}{3}$. It remains conceivable, however, that smaller values of β^2 can be reached in the model (1) in the limit $E_c = \Delta \ll t$.

V. EXCITON PROPERTIES

In Wannier theory¹ exciton properties, such as size, binding energy, effective mass, or optical weight, are related by simple equations and exhibit a monotonic behavior as a function of the Coulomb repulsion strength. This simplicity is due to a drastic assumption of this theory: optical excitations are represented by an electron (in the conduction band) and a hole (in the valence band), which are completely independent from the system's other degrees of freedom. The interaction with these degrees of freedom is taken into account only through renormalized parameters such as effective masses for the electron and hole, and an effective background dielectric constant for the Coulomb interaction between electron and hole.

In a Mott insulator the exciton properties show a more complex behavior. Although a Mott-Hubbard exciton can also be described as a bound pair of excitations with opposite charges, the Coulomb interaction at the same time determines the size of the Mott gap, the exciton properties, and the coupling of the exciton to the other electrons in the system. Therefore, an increase of the Coulomb interaction strength does not simply bind the exciton more tightly, but also renormalizes the gap and couples the particle-hole excitation more strongly to the other electrons. This leads to a non-monotonic behavior of Mott-Hubbard exciton properties as a function of the Coulomb repulsion strength, and even to an instability toward the formation of excitonic strings or charge-density-wave droplets¹⁷.

In the following two subsections we shall discuss the binding energy and size of a Mott-Hubbard exciton using analytical results in the limits of large and small Mott gaps, and numerical results in the intermediate regime.

A. Binding energy

The exciton binding energy is usually defined as the energy difference between the exciton ω_{ex} and the band edge of the particle-hole continuum E_c

$$\delta E = E_c - \omega_{\text{ex}}. \quad (45)$$

In Wannier theory this quantity is the energy required to break an exciton into independent hole and electron.

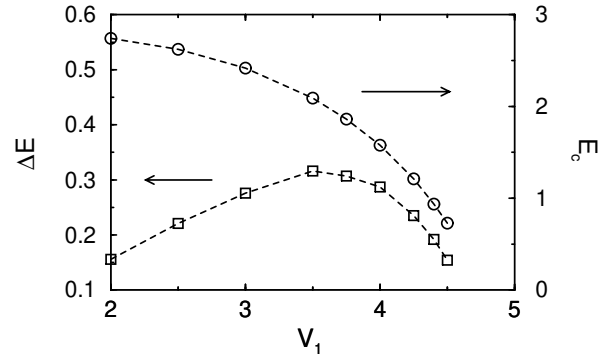


FIG. 4. Charge gap E_c (circles, right axis) and exciton binding energy δE (squares, left axis) as a function of V_1 for $U = 6t$ and $V_2 = 2t$.

In a Mott insulator this is not always warranted as δE does not necessarily correspond to the minimal energy required to break an exciton. For instance, as seen in (9b), there is an exciton *above* the band edge in the strong-coupling limit $U \gg 4t > V_1$ ($V_2 = 0$). Except for this strong-coupling limit, however, we have only found excitons with an energy ω_{ex} lower than the absorption band edge E_c in our study of the model (1). Therefore, we assume that δE is indeed the binding energy of the single Mott-Hubbard exciton observed in the spectrum of the Mott-insulating phase of (1).

In the limit of a large Mott gap ($U \gg t, V_1, V_2$) $\delta E = V_1 + 4t^2/V_1 - 4t$ for $V_1 \geq 2t$ and $V_2 = 0$, see (9a). The binding energy increases monotonically with V_1 but, clearly, it is not a good measure for the strength of the Coulomb interaction as it is independent of U and vanishes even when V_1 is still quite strong ($V_1 = 2t$). For intermediate Mott gaps ($0.1 \leq E_c/4t \leq 10$) we have found that the binding energies (ranging from $0.03t$ to $12t$) do not depend in a simple way on the Coulomb interaction strength. In particular, δE has a non-monotonic behavior as illustrated in Fig. 4. The binding energy δE first increases with V_1 as long as the gap E_c remains essentially unchanged, then δE and E_c decrease rapidly as V_1 approaches the critical surface $U - 2V_1 + 2V_2 \approx 0$. It is likely that the same behavior also holds for small Mott gaps ($E_c = \Delta \ll t$), where field theory gives $\delta E = \Delta(1 - \sin(\pi\xi/2))$, $\xi \leq 1$, for the first exciton, see (23). If we take the weak-coupling result (16) as an indication of the qualitative dependence of β on V_1 , then an increase of V_1 leads to smaller ξ , (24), and thus to a larger binding energy. On the other hand, an increase of V_1 can also lead to a sharp *decrease* of the gap Δ close to the critical surface $U - 2V_1 + 2V_2 \approx 0$, if we again take the weak-coupling results (20) and (21) to be indicative of the qualitative dependence of Δ on V_1 . Depending on the other parameter values, one of these two effects dominates and leads to an increase or decrease of the binding energy when V_1 becomes larger.

In summary, our analysis shows that the binding energy of a Mott-Hubbard exciton does not provide a good

estimate of the Coulomb interaction strength in a Mott insulator. Of course, a large gap E_c or binding energy δE requires a strong Coulomb interaction. In general, however, a small E_c or δE are *not* an indication for a weak electron-electron interaction. In contrast to the views of Ref. 37, even a “small” exciton binding energy, of the order of 0.1 eV in some π -conjugated systems, does *not* imply that electron-electron interactions are small in these materials.

B. Size

In the limit of large Mott gaps ($U \gg t, V_1, V_2$) an optical excitation is simply made of a hole and a double occupancy in a background of singly occupied sites (Sec. III A). The probability of finding the hole and double occupancy at a distance x in an optical excitation is given by the correlation function

$$C_{\text{hd}}(x) = \langle \hat{n}_{l,\uparrow} \hat{n}_{l,\downarrow} (1 - \hat{n}_{l+x,\uparrow}) (1 - \hat{n}_{l+x,\downarrow}) \rangle, \quad (46)$$

where $\langle \dots \rangle$ means the expectation value in the corresponding excited N -electron eigenstate. The average distance between hole and double occupancy is

$$\zeta_{\text{hd}} = \frac{\sum_x C_{\text{hd}}(x) |x|}{\sum_x C_{\text{hd}}(x)}. \quad (47)$$

If the hole and double occupancy are not bound, this quantity diverges as the system size L goes to infinity. For an exciton, ζ_{hd} remains finite as $L \rightarrow \infty$ and can be interpreted as the exciton size. For $V_1 \geq 2t$ and $V_2 = 0$ an analytical calculation gives the exact result

$$C_{\text{hd}}(x \neq 0) \propto \exp(-\kappa |x|) \quad (48)$$

with $\kappa = 2 \ln(V_1/2t)$ for the lowest exciton. The exciton size is then

$$\zeta_{\text{hd}} = \frac{1}{1 - e^{-\kappa}} \quad (49a)$$

$$= \frac{1}{1 - (2t/V_1)^2}. \quad (49b)$$

ζ_{hd} diverges as V_1 approaches the critical value ($V_c = 2t$), below which the pair is not bound, and tends to unity for strong coupling, $V_1/2t \rightarrow \infty$. Using a density-density correlation function^{9,10} yields equivalent results.

Unfortunately, the correlation function for hole and double occupancy and the density-density correlation functions yield unclear results in the regime of intermediate Mott gaps because the ground state already contains a finite density of holes and double occupancies when E_c/t is finite. The function (46), for instance, tends to a finite value d^2 as $x \rightarrow \infty$, which is determined by the density of doubly occupied sites $d = \langle \hat{n}_{l,\uparrow} \hat{n}_{l,\downarrow} \rangle$. These quantum charge fluctuations hide the weak exciton contribution to (46).

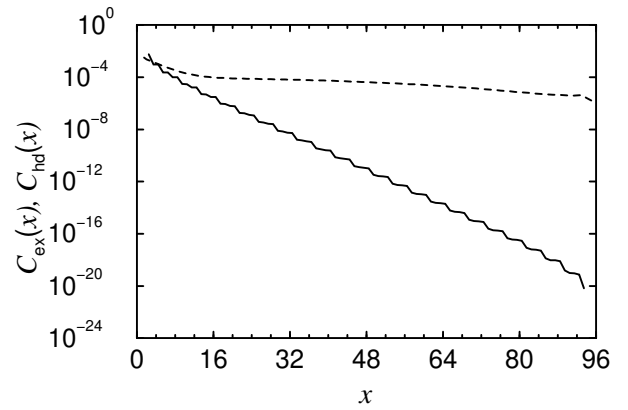


FIG. 5. Correlation functions for a hole and double occupancy, $C_{\text{hd}}(x)$ (dashed), and for an electron-hole excitation, $C_{\text{eh}}(x)$ (solid), calculated for the lowest exciton in a 96-site system with $U = 40t$, $V_1 = 2.5t$, and $V_2 = 0$. The center of the pair is in the middle of the lattice.

In Fig. 5 we show the correlation function $C_{\text{hd}}(x)$ calculated with DMRG for the lowest optically excited state in the model (1) with $U = 40t$, $V_1 = 2.5t$, and $V_2 = 0$. This system is in the regime of large Mott gaps with $E_c \approx 36.14t$, and is well described by our strong-coupling analysis, which predicts an exciton with a size $\zeta_{\text{hd}} \approx 2.78$ as the lowest optically excited state. However, one clearly sees in Fig. 5 that $C_{\text{hd}}(x)$ remains finite for large x . This wrongly suggests that the optically generated hole and double occupancy are not bound in this excited state. Similar problems arise with a density-density correlation function. Taking the difference between the correlation functions for an excited state and for the ground state, as in Ref. 10, does not provide better results.

A suitable quantity for our analysis is the correlation function for electron-hole excitations

$$C_{\text{eh}}(x) = \left| \left\langle n \left| \hat{P}_{l,l+x} + (-1)^{|x|} \hat{P}_{l+x,l} \right| 0 \right\rangle \right|^2, \quad (50)$$

where $|0\rangle$ is the ground state, $|n\rangle$ is the excited state under investigation, and

$$\hat{P}_{i,j} = \sum_{\sigma} \hat{c}_{i,\sigma}^+ \hat{c}_{j,\sigma} \quad (51)$$

creates an electron at site i and a hole at site j . Obviously, $C_{\text{eh}}(x)$ evaluates the importance of an electron-hole excitation with distance x in the excited state $|n\rangle$. This approach has already been used to study the structure of excited states in semiempirical calculations for ladder-type PPP oligomers³⁸. Here, we have calculated this correlation function using the symmetrized DMRG method to analyze the structure of excited states in the lattice model (1).

An average electron-hole distance ζ_{eh} can be defined by substituting $C_{\text{eh}}(x)$ for $C_{\text{hd}}(x)$ in Eq. (47). We have

found that this method predicts correctly whether a hole-double occupancy pair is bound or unbound in the limit of large Mott gaps ($U \gg t, V_1, V_2$). The advantage of the correlation function $C_{\text{eh}}(x)$ over $C_{\text{hd}}(x)$ (or a density-density correlation function) becomes obvious in a system with a *finite* Mott gap. In Fig. 5 one sees that $C_{\text{eh}}(x)$ decreases exponentially and thus allows us to identify a bound excitation, while the correlation function between hole and double occupancy $C_{\text{hd}}(x)$ is dominated by the finite ground-state density of holes and double occupancies. Therefore, we think that the correlation function for electron-hole excitations $C_{\text{eh}}(x)$ and the analysis of the average electron-hole distance ζ_{eh} provide a reliable approach to distinguish an exciton from an unbound particle-hole excitation in correlated systems. In any case, this approach is more reliable than schemes based on the correlation function for hole and double occupancy or a density-density correlation function.

However, this approach cannot be used to determine the size of a bound pair accurately because $C_{\text{eh}}(x)$ is affected by very strong short-range fluctuations due to spin correlations and lattice and chain-end effects. [In our figures we show a running average of $C_{\text{eh}}(x)$.] Instead, we evaluate the exciton size ζ_{ex} as the average electron-hole distance [as in Eq. (47)] calculated for the exponential function which gives the best fit to $C_{\text{eh}}(x)$

$$C_{\text{eh}}(x) \propto \exp(-\lambda|x|), \quad (52a)$$

$$\zeta_{\text{ex}} = \frac{1}{1 - \exp(-\lambda)}. \quad (52b)$$

In the limit of large Mott gaps we have found that this approach reproduces the exact result (49b) for the exciton size, i.e., $\zeta_{\text{ex}} \approx \zeta_{\text{hd}}$. Furthermore, applying this analysis to systems with large but finite gaps yields results in agreement with our strong-coupling analysis. For instance, using the data for $U = 40t$ and $V_1 = 2.5t$ in Fig. 5 our analysis gives $\zeta_{\text{ex}} = 2.99$. This value agrees within 10% with the analytical result (49b) for $U/t \rightarrow \infty$ and $V_1 = 2.5t$, $\zeta_{\text{hd}} = 2.78$. The difference can be explained as a correction of the order $4t/U$. Therefore, we think that the analysis (52) of the correlation function for electron-hole excitations allows one to determine reliably the size of an exciton in a correlated system.

We have calculated the average electron-hole distance ζ_{eh} of the lowest optically excited states for various values of the parameters U , V_1 , and V_2 in the regime of intermediate Mott gaps. The analysis of ζ_{eh} yields predictions about the presence of bound particle-hole pairs which always agree with the predictions based on the analysis of the excited-state energies. For an excited state above the absorption band threshold we have found that ζ_{eh} diverges with system size, confirming that this excitation is made of an unbound particle-hole pair. A representative example for the various possible shapes of $C_{\text{eh}}(x)$ is shown in Fig. 6. For an unbound pair one clearly sees that $C_{\text{eh}}(x)$ remains finite for very large x of the order of the system size L . $C_{\text{eh}}(x)$ only goes to zero as x approaches

the system size ($L = 256$ in this example) because of chain-end effects.

In contrast, when an excited state lies below the charge gap E_c , we have found that ζ_{eh} remains finite for an infinite system, confirming that this excited state is made of a bound particle-hole pair (exciton). In this case, $C_{\text{eh}}(x)$ decreases exponentially and we can use the analysis (52) to determine the exciton size ζ_{ex} . A typical example is also shown in Fig. 6. We note that both examples in Fig. 6 correspond to systems with a gap $E_c \approx 0.66t$, for which the field theory of Sec. IV is still valid and supports our identification of bound and unbound excitations.

The exciton sizes ζ_{ex} observed range from slightly more than one lattice spacing a_0 to about $20a_0$. As the binding energy δE , the exciton size ζ_{ex} does not depend in a simple way on the Coulomb interaction strength and even displays a non-monotonic behavior as a function of V_1 , first decreasing as V_1 increases, then sharply increasing as V_1 approaches the critical regime $U - 2V_1 + 2V_2 \approx 0$. As expected, ζ_{ex} becomes larger and seems to diverge as δE vanishes, while it diminishes when δE becomes larger if the gap E_c is kept (approximately) constant.

We note that the operator used in (50) is antisymmetric with respect to charge conjugation, as is the current operator (3). Thus, $C_{\text{eh}}(x)$ is non-zero only for those excited states $|n\rangle$ (including the excited states contributing to the linear optical conductivity) whose parity P_c under charge conjugation is opposite to that of the ground state. When a minus sign is substituted for the + sign in (50), $C_{\text{eh}}(x)$ is non-zero for excited states which have the same parity under charge conjugation as the ground state. One can thus extend this scheme to excited states which contribute to the non-linear optical properties of a system.

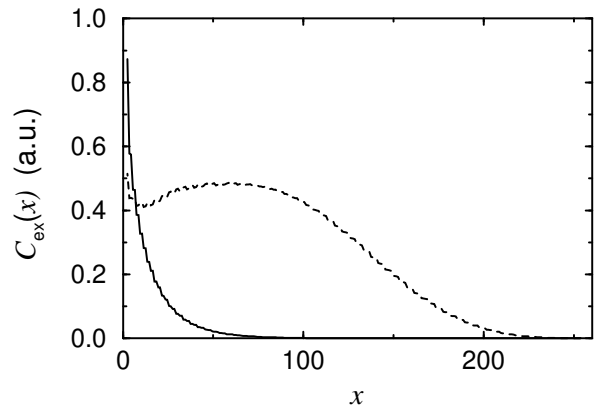


FIG. 6. Correlation function $C_{\text{eh}}(x)$ of the first optically excited state on a 256-site lattice for two typical cases: an exciton (solid) for $U = 4t$, $V_1 = 2.75t$, and $V_2 = 1.5t$, and an unbound particle-hole pair (dashed) for $U = 3.5t$, $V_1 = 1.4t$, and $V_2 = 0$. The center of the pair is in the middle of the lattice.

In the field-theory limit, a measure of the size of an exciton can be obtained in the following way. For asymp-

totically large separation between particles, the holon-antiholon wave function has the form

$$\begin{aligned}\Psi_{x_1 \ll x_2}(x_1, x_2) &= \exp(ip_1 x_1 + ip_2 x_2) \\ &\quad + S_R(p_1, p_2) \exp(ip_2 x_1 + ip_1 x_2), \\ \Psi_{x_1 \gg x_2}(x_1, x_2) &= S_T(p_1, p_2) \exp(ip_1 x_1 + ip_2 x_2),\end{aligned}\quad (53)$$

where $S_{R,T}$ are two-particle S -matrix elements corresponding to reflection and transmission respectively. In terms of rapidity variables defined by $p_j = M \sinh \theta_j / v_c$, the S -matrix only depends on the difference $\theta_{12} = \theta_1 - \theta_2$ and has poles at

$$\theta_{12} = i\pi(1 - n\xi). \quad (54)$$

An exciton state with energy $M_n \cosh \theta$ and momentum $M_n \sinh \theta / v_c$ is obtained by choosing

$$\begin{aligned}p_1 &= \frac{M}{v_c} \sinh\left(\theta + i\frac{\pi - \pi n\xi}{2}\right), \\ p_2 &= \frac{M}{v_c} \sinh\left(\theta - i\frac{\pi - \pi n\xi}{2}\right).\end{aligned}\quad (55)$$

Inserting these values in the wave function yields an exponential decay in $|x_2 - x_1|$ with correlation length

$$\zeta_n^{\text{FT}} = \frac{v_c}{M \cos \pi n\xi / 2}, \quad (56a)$$

$$= \frac{2v_c}{\sqrt{\Delta^2 - M_n^2}}. \quad (56b)$$

We see that this size diverges when we approach from below the coupling constant ξ , at which the n -th exciton is first formed. For example, the first exciton splits off the holon-antiholon continuum at $\xi = 1$ and its size displays a square-root divergence for $\xi \rightarrow 1$

$$\zeta_1^{\text{FT}} \propto \sqrt{\frac{1}{\Delta - M_1}} \quad ; \quad M_1 \rightarrow \Delta^- . \quad (57)$$

The non-monotonic behavior of the exciton size as a function of the Coulomb interaction strength is also observed in the small-gap regime. Equation (56a) shows that ζ_1^{FT} will decrease if the diminution of ξ dominates when the lattice parameter V_1 increases, but becomes greater if the increase of the velocity v_c and the reduction of the gap Δ prevail (see Sec. IV).

To compare the field-theoretical predictions with our numerical method based on the correlation function $C_{\text{eh}}(x)$ we have numerically calculated the exciton energy ω_{ex} and size ζ_{ex} for several values of the parameters U , V_1 , and V_2 , corresponding to gaps $\Delta = E_c$ of the order of $0.6t$. The exciton sizes range from $10a_0$ to $20a_0$. We have found that in all cases our numerical results fulfill the field-theory relation (56b) within 15% if we use $v_c = 2ta_0$ as the charge velocity. This good agreement shows that our definitions (52) and (56) are mutually consistent in the regime of small Mott gaps. Moreover, the numerical method yields reasonable estimates of the exciton size even in the regime where such calculations become laborious.

VI. CONCLUSIONS

We have investigated excitons in the optical conductivity spectrum of one-dimensional Mott insulators using two new reliable methods, the dynamical density-matrix renormalization group and the field-theoretical form-factor bootstrap approach, supplemented by two established techniques, a strong-coupling analysis and the symmetrized DMRG. Mott-Hubbard excitons can be understood with the simple picture of a bound pair of spinless bosonic excitations with opposite charge, in analogy to the bound electron-hole pair of Wannier exciton theory. However, the properties of Mott-Hubbard excitons are not as simple as those of Wannier excitons because both the Mott gap and the force between charged excitations originate from the Coulomb repulsion between electrons and are thus interdependent. In particular, the smallness of an exciton binding energy is no indication for the strength of the Coulomb repulsion in a Mott insulator.

We may compare our results to experiments for polydiacetylene chains in their monomer matrix. For an estimate of the exciton size we use the field-theoretical result (56) which is fairly independent of the details of the lattice structure and the range of the electron-electron interaction. We put $v_c \approx v_F = 2ta_0$ with a π -electron band width $W = 4t \approx 10 \text{ eV}$ ³⁹, $\Delta = \omega_{\text{ph}} = 2.4 \text{ eV}$, and $M_1 = \omega_{\text{ex}} = 1.9 \text{ eV}$ from experiment for 3BCMU-PDA⁵. The field-theoretical prediction for the exciton size,

$$\zeta_1^{\text{FT}} = a_0 \frac{W}{\sqrt{\omega_{\text{ph}}^2 - \omega_{\text{ex}}^2}} \approx 7a_0 \approx 9 \text{ \AA} \quad (58)$$

is in fair agreement with the experimental value 12 \AA if we put $a_0 = 1.3 \text{ \AA}$ for the average bond length between the carbon atoms on the PDA chain. The difference can be attributed to the limitations of this simple calculation or the uncertainty of the order of 20% for the experimental values⁴⁰. We therefore conclude that our many-body approach can be applied successfully to real polymers.

Although the particular model studied here is too simple to describe conjugated polymers accurately, we believe that the concept of Mott-Hubbard excitons is relevant for these materials as the electron-electron interaction significantly contributes to the formation of their optical gap. In any case, this approach is more realistic than the oversimplified Wannier theory and other simple approaches that neglect or minimize the role of electronic correlations in conjugated polymers. The many-body methods used in this work can be applied (and in part, have already been applied) to more realistic models taking into account the polymer geometrical structure

and the electron-phonon interaction, and possibly additional perturbations such as interchain couplings. We think that the optical properties of conjugated polymers will be successfully investigated using a combination of these many-body methods.

ACKNOWLEDGMENTS

We gratefully acknowledge helpful discussions with R. Bursill and G. Weiser.

-
- ¹ See, e.g., H. Haug and S.W. Koch, *Quantum Theory of the Optical and Electronic Properties of Semiconductors* (World Scientific, Singapore, 1990).
 - ² *Organic Conductors*, ed. by J.-P. Farges (Marcel Dekker, New York, 1994).
 - ³ D. Baeriswyl, D.K. Campbell, and S. Mazumdar in *Conjugated Conducting Polymers*, ed. by H. Kiess (Springer, Berlin, 1992).
 - ⁴ L. Sebastian and G. Weiser, Phys. Rev. Lett. **46**, 1156 (1981).
 - ⁵ A. Horváth, G. Weiser, C. Lapersonne-Meyer, M. Schott, and S. Spagnoli, Phys. Rev. B **53**, 13507 (1996).
 - ⁶ The present status of the discussion is summarized in *Primary Photoexcitations in Conjugated Polymers: Molecular Exciton versus Semiconductor Band Model*, ed. by N.S. Sariciftci (World Scientific, Singapore, 1999).
 - ⁷ A.J. Heeger, S. Kivelson, J.R. Schrieffer, and W.P. Su, Rev. Mod. Phys. **60**, 781 (1988).
 - ⁸ S. Abe, J. Yu and W.P. Su, Phys. Rev. B **45**, 8264 (1992); S. Abe, M. Schreiber, W.P. Su and J. Yu, *ibid.*, 9432 (1992); M.J. Rice and Yu N. Garstein, Phys. Rev. Lett. **73**, 2504 (1994).
 - ⁹ D. Guo, S. Mazumdar, S.N. Dixit, F. Kajzar, F. Jarka, Y. Kawabe, and N. Peyghambarian, Phys. Rev. B. **48**, 1433 (1993); F. Guo, D. Guo, and S. Mazumdar, Phys. Rev. B. **49**, 10102 (1994).
 - ¹⁰ M. Boman and R.J. Bursill, Phys. Rev. B. **57**, 15167 (1998); R.J. Bursill and W. Barford, Phys. Rev. Lett. **82**, 1514 (1999).
 - ¹¹ Z. Shuai, S.K. Pati, W.P. Su, J.L. Brédas, and S. Ramasesha, Phys. Rev. B **55**, 15368 (1997).
 - ¹² S.K. Pati, S. Ramasesha, Z. Shuai, and J.L. Brédas, Phys. Rev. B **59**, 14827 (1999); S. Ramasesha, S.K. Pati, H.R. Krishnamurthy, Z. Shuai, and J.L. Brédas, Synth. Met. **85**, 1019 (1997).
 - ¹³ N.F. Mott, *Metal-Insulator Transitions*, 2nd ed. (Taylor and Francis, London, 1990); F. Gebhard, *The Mott Metal-Insulator Transition* (Springer, Berlin, 1997).
 - ¹⁴ E. Jeckelmann, F. Gebhard and F.H.L. Essler, Phys. Rev. Lett. **85**, 3910 (2000).
 - ¹⁵ F. Gebhard, K. Bott, M. Scheidler, P. Thomas, and S.W. Koch, Phil. Mag. B **75**, 1, 13, 47 (1997).
 - ¹⁶ J. Hubbard, Proc. R. Soc. London A **276**, 238 (1963).
 - ¹⁷ E. Jeckelmann, *Optical excitations in the Mott insulator phase of the one-dimensional extended Hubbard model* (in preparation).
 - ¹⁸ S.R. White, Phys. Rev. Lett. **69**, 2863 (1992); Phys. Rev. B **48**, 10345 (1993).
 - ¹⁹ *Density-Matrix Renormalization*, I. Peschel, X. Wang, M. Kaulke, and K. Hallberg (editors) (Springer, Berlin, 1999).
 - ²⁰ T.D. Kühner and S.R. White, Phys. Rev. B **60**, 335 (1999).
 - ²¹ E. Jeckelmann (in preparation).
 - ²² S. Ramasesha, S.K. Pati, H.R. Krishnamurthy, Z. Shuai, and J.L. Brédas, Phys. Rev. B. **54**, 7598 (1996).
 - ²³ F.B. Gallagher and S. Mazumdar, Phys. Rev. B. **56**, 15025 (1997).
 - ²⁴ S.S. Kancharla and C.J. Bolech (unpublished; preprint cond-mat/0012443).
 - ²⁵ Z. Shuai, J.L. Brédas, S.K. Pati, and S. Ramasesha, Phys. Rev. B **58**, 15329 (1998).
 - ²⁶ This was first noticed by Robert Bursill for excitons in the extended Hubbard model with alternating hopping integrals (private communication); see also Ref. 10.
 - ²⁷ A.O. Gogolin, A.A. Nersesyan, and A.M. Tsvelik, *Bosonization in Strongly Correlated Systems* (Cambridge University Press, Cambridge, 1999).
 - ²⁸ D. Controzzi, F.H.L. Essler, and A.M. Tsvelik, proceedings of the NATO ASI/EC summer school *New Theoretical Approaches to Strongly Correlated Systems*, Cambridge 2000 (preprint cond-mat/0011439).
 - ²⁹ A. Luther, Phys. Rev. B **14**, 2153 (1976); A.B. Zamolodchikov and A.I.B. Zamolodchikov, Ann. Phys. **120**, 253 (1979); H. Bergknoff and H. Thacker, Phys. Rev. D **19**, 3666 (1979); V.E. Korepin, Theor. Math. Phys. **41**, 169 (1979).
 - ³⁰ D. Controzzi, F.H.L. Essler, and A.M. Tsvelik, Phys. Rev. Lett. **86**, 960 (2001).
 - ³¹ O.J. Heilmann and E.H. Lieb, Ann. N.Y. Acad. Sci. **172**, 583 (1971); C.N. Yang, Phys. Rev. Lett. **63**, 2144 (1989).
 - ³² F.A. Smirnov, *Form Factors in Completely Integrable Models of Quantum Field Theory* (World Scientific, Singapore, 1992).
 - ³³ M. Karowski and P. Weisz, Nucl. Phys. **B139**, 455 (1978); H. Babujian, A. Fring, M. Karowski, and A. Zapletal, Nucl. Phys. **B538**, 535 (1999); S. Lukyanov, Comm. Math. Phys. **167**, 183 (1995); S. Lukyanov, Mod. Phys. Lett. A **12**, 2911 (1997); S. Lukyanov and A. Zamolodchikov, hep-th/0102079; A. Fring, G. Mussardo, and P. Simonetti, Nucl. Phys. **B393**, 413 (1993).
 - ³⁴ A.B. Zamolodchikov, JETP Lett. **25**, 468 (1977); H.-J. Thun, T.T. Truong, P.H. Weisz, Phys. Lett. **B67**, 321 (1977).
 - ³⁵ J. Cardy and G. Mussardo, Nucl. Phys. **B410**, 451 (1993).
 - ³⁶ G. Mussardo (unpublished; preprint hep-th/940512).
 - ³⁷ A.J. Heeger in Ref. 6, p. 20.
 - ³⁸ J. Rissler, F. Gebhard, H. Bässler, and P. Schwerdtfeger (unpublished; preprint cond-mat/0103320).
 - ³⁹ W.R. Salaneck, M. Fahlman, C. Lapersonne-Meyer, J.-L. Fave, M. Schott, M. Lögdlund, and J.L. Brédas, Synth. Met. **67**, 309 (1994).
 - ⁴⁰ G. Weiser, private communication (2000).